THE JOURNAL OF PHYSICAL CHEMISTRY A LETTERS

2006, *110,* 7989−7993
Published on Web 06/15/2006

Vibrational and Vibronic Processes in Coherent 2D Resonance Raman Spectroscopy

Peter C. Chen* and Candace C. Joyner

Spelman College Chemistry Department, 350 Spelman Lane, Atlanta, Georgia 30314

Received: March 30, 2006; In Final Form: May 20, 2006

Coherent 2D resonance Raman spectroscopy is a multidimensional technique that is capable of separating and sorting peaks that appear heavily congested and disordered in conventional 1D spectra. It can sort rovibrational peaks according to rotational and vibrational quantum number, vibrational sequence, and rotational selection rule. New results suggest that pattern recognition methods can also be used to determine whether the highly detailed rovibrational information is coming from the ground electronic state or the excited electronic state. This capability is demonstrated using experimental results from I_2 and C_2.

Coherent 2D resonance Raman spectroscopy (C2DRRS) is a new technique that uses the coupling between rovibrational levels in different electronic states to separate and sort congested peaks in gas-phase electronic spectroscopy.[1] Like other two-dimensional forms of spectroscopy,[2−11] C2DRRS can improve spectral resolution as it spreads the peaks across the second dimension and displays coupled peaks in the off-diagonal regions of the spectrum. A traditional challenge for conventional gas-phase spectroscopy has been that large numbers of rovibrational peaks from different processes often overlap, resulting in congestion and the appearance of disorder. A recent paper[1] describes the ability of C2DRRS to also sort congested and disordered rovibrational peaks from C_2 into patterns of neighboring parabolas according to rotational and vibrational quantum number, sequence, and selection rule. Unlike conventional 1D emission spectra, where transitions can originate from any level in the excited state, the C2DRRS four-wave mixing process employs rules that are more restrictive. In the case of the C2DRRS results from C_2, each peak in the resulting 2D spectrum is attributed to a pair of ground-state rovibrational levels that are each coupled (by a single photon) to a common level in the excited state. As a result, all peaks within a given parabola have the same rotational selection rule, have the same vibrational quantum numbers (and vibrational sequence), and are ordered by rotational quantum number.

The demonstrated ability to sort peaks in C_2 raises the question of how to use and interpret C2DRRS spectra for general application. One particularly relevant issue is the existence of differing four-wave mixing processes. The existence of multiple-wave mixing processes has been well studied and is responsible for effects such as pressure and dephasing-induced extra resonances.[12,13] In conventional 1D spectroscopy, the determination and identification of multiple processes usually requires an investigation that involves additional experimentation and modeling. For example, Hogervorst and co-workers recently used a combination of broadband and narrowband lasers to discern excited-state parametric CARS from two other processes in I_2.[14] For resonantly enhanced coherent Raman spectroscopy, peaks can generally be produced by processes that involve rovibrational levels in the ground state and by processes that involve rovibrational levels in excited electronic states.

This paper describes the use of pattern recognition as a means for distinguishing multiple processes in C2DRRS spectroscopy. Figure 1 shows the energy level diagrams for two different types of doubly resonant C2DRRS four-wave mixing processes. Levels a and b are in the ground electronic state, levels c and d are in the excited electronic state, and level e represents a virtual level. Input frequencies ω_1 and ω_2 are generated by broadband near-infrared beams that together induce Raman-type resonances. The >3000 cm^{-1} range covered by these broadband beams ensures that all Raman-active rovibrational levels are probed simultaneously. Input frequency ω_3 comes from a tunable narrowband visible or UV input beam that induces a resonance between the ground and excited electronic states.

The Raman-type interaction (from $\omega_1 - \omega_2$) for the first process in Figure 1 probes vibrational levels in the ground electronic state. In contrast, the second process probes vibronic levels (the Raman-active vibrations are in the excited electronic state). To produce an experimental C2DRRS spectrum, intensity ($I \approx |\chi^{(3)}|^2$) is recorded as a function of both ω_3 (y axis) and ω_4 (x axis). The equations describing the nonlinear susceptibility of these two doubly resonant processes are

$$\chi^{(3)}_{\text{vibrational}} \propto \Sigma\, \mu_{ae}\mu_{eb}\mu_{bd}\mu_{da}/\Delta_{ea}\,\Delta_{ba}\,\Delta_{da}$$

$$\chi^{(3)}_{\text{vibronic}} \propto \Sigma\, \mu_{ac}\mu_{ce}\mu_{ed}\mu_{da}/\Delta_{ca}\,\Delta_{ea}\,\Delta_{da}$$

where

$$\Delta_{da} = \omega_{da} - (\omega_1 - \omega_2 + \omega_3) - i\Gamma_{da}$$

$$\Delta_{ba} = \omega_{ba} - (\omega_1 - \omega_2) - i\Gamma_{ba}$$

$$\Delta_{ca} = \omega_{ca} - \omega_3 - i\Gamma_{ca}$$

and

$$\Delta_{ea} = \omega_{ea} - \omega_1 - i\Gamma_{ea}$$

* Corresponding author. E-mail: pchen@spelman.edu; Fax: 404-270-5752.

10.1021/jp061983a CCC: $33.50 © 2006 American Chemical Society

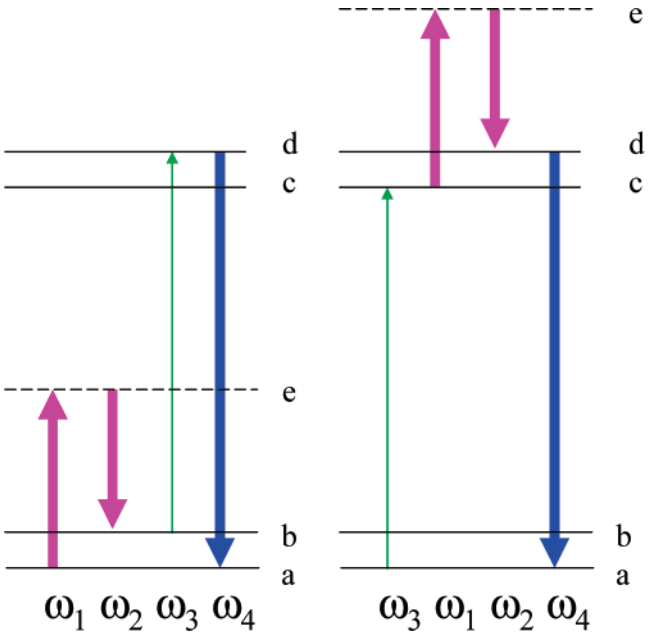

Figure 1. Energy level diagrams for both the vibrational (left) and vibronic (right) processes. The wider arrows represent broadband beams.

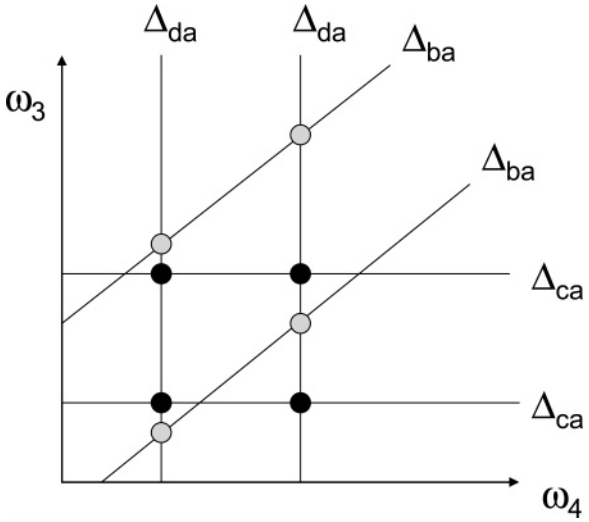

Figure 2. Simulated horizontal, vertical, and diagonal resonance lines and their points of intersection that produce a repeating rectangular vibronic pattern (dark circles) and/or a repeating parallelogram vibrational pattern (light circles).

for the vibrational process, but

$$\Delta_{ea} = \omega_{ea} - (\omega_3 + \omega_1) - i\Gamma_{ea}$$

for the vibronic process. The difference between the two Δ_{ea} terms is of little concern because level e is nonresonant. A more important difference is that Δ_{ca}, which varies with ω_3 only, is part of the vibronic expression but not the vibrational expression.

For simple diatomic molecules, the frequencies of the states (ω_{ba}, ω_{ca}, etc.) can be determined using the conventional expressions for the sum of electronic, vibrational, and rotational energies.[1] Simulations indicate that the shape of the parabolas is largely controlled by the rotational spectroscopic constants, while the location is primarily affected by the electronic and vibrational constants.[15] Therefore, neglecting rotational terms, the (x,y) location of these parabolas for the vibrational process is given by

$$(\omega_4, \omega_3) = (\Delta T_e + G'_d - G''_a, \Delta T_e + G'_d - G''_b)$$

and the location for the vibronic process is

$$(\omega_4, \omega_3) = (\Delta T_e + G'_d - G''_a, \Delta T_e + G'_c - G''_a)$$

Here, G'_d is the vibrational energy corresponding to level d (in the excited electronic state), G''_a is the vibrational energy corresponding to level a (in the ground electronic state), and $\Delta T_e = T_e' - T_e''$. The ω_4 values for both processes are identical, but the ω_3 values are not. For the vibronic process, c and d can be any vibronic level, so the set of possible ω_3 values is the same as the set of possible ω_4 values. This result suggests a similarity between spacings on the x axis and spacings on the y axis for the vibronic process. However, the value for $G'_c - G''_a$ is generally different from $G'_d - G''_b$ except in the rare situation when $\omega_e' = \omega_e''$. Therefore, the same type of pattern should not normally be observed for the vibrational process.

Further insight into the location of both singly and doubly resonant contributions can be made by plotting resonance lines in 2D space (see Figure 2). Singly resonant processes produce horizontal (Δ_{ca}), vertical (Δ_{da}), and diagonal (Δ_{ba}) resonance lines when plotted in 2D frequency or energy space. More intense than these singly resonant lines will be the doubly resonant points that occur where the singly resonant lines intersect. For the vibronic process, the intersection points (dark circles) should occur between horizontal Δ_{ca} resonance lines and vertical Δ_{da} resonance lines. The complete set of vibronic levels includes both the fundamental and overtones. The resulting vibronic process produces a frame of cross-peaks that resembles a rectangular grid. On the other hand, the vibrational process contains Δ_{ba} and Δ_{da}, and therefore has doubly resonant cross-peaks (light circles) where diagonal resonance lines cross the vertical resonance lines. Vibrational overtones are also commonly observed in resonance Raman spectroscopy. The vibrational process therefore should produce a frame of cross-peaks that align vertically but not horizontally (i.e., they form a parallelogram rather than a rectangular grid). Each doubly resonant cross-peak consists of a series of two (or more) intersecting parabolas, with its location defined by the point where these parabolas intersect.[15]

On the Stokes side (not commonly used due to the increased potential for spectral interference from incoherent luminescence), the processes should be symmetric to the anti-Stokes side with respect to the diagonal $\omega_3 = \omega_4$. Therefore, the pattern on the anti-Stokes side should be mirrored (in frequency space) by the process on the Stokes side. For the vibronic process, however, the pattern is unchanged on either side of the diagonal. For the vibrational process, the diagonal lines retain a slope of 1 (if plotted in the frequency or energy domain), but the lines that were vertical on the anti-Stokes side should convert to horizontal lines on the Stokes side.

Both processes should reveal information about the relationship between spectroscopic peaks (i.e., what peaks are coupled to a common level through interaction with a photon). As mentioned before, the vibrational process reveals peaks in (ω_4, ω_3) space from two vibrational levels (a and b) that are each coupled by a single photon (either ω_3 or ω_4) to a common level in the excited electronic state (level d). Therefore, the vibrational process reveals "coupled" emission peaks. On the other hand, the vibronic process reveals peaks from two vibronic levels (c and d) that are each coupled by a single photon (either ω_3 or

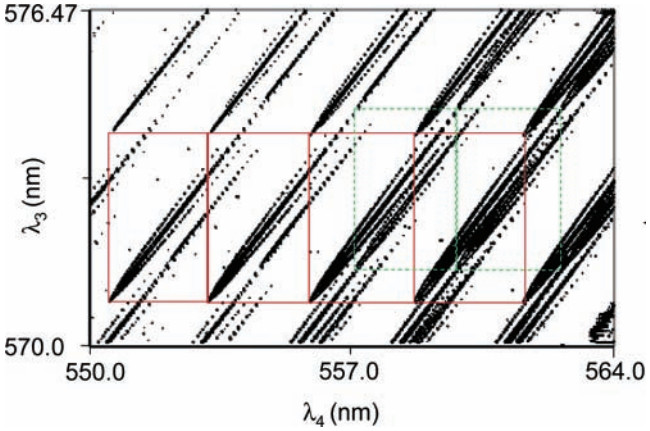

Figure 3. Experimental C2DRRS spectrum of I_2. The corners of the (red) solid line boxes mark vibronic processes that start from $v'' = 0$, while those of the (green) broken line boxes indicate vibronic processes that start from $v'' = 1$.

ω_4) to a common level in the ground electronic state (level a). Therefore, the vibronic process reveals "coupled" absorption peaks.

Experimental Section

The C2DRRS setup for C_2 has been described previously.[1] C2DRRS spectra of I_2 were recorded using the same laser system but a different detection system (1.25 m Czerny−Turner SPEX 1250m monochromator equipped with a 1200 g/mm grating and a Spectrum One 2048 × 512 CCD, pixel width of 13.5 μm). The quartz sample cell (cylindrical, 1 in. diameter and 4 in. long) contained saturated iodine vapor at 23 °C. Both BOXCARS phasematching (similar to that used in ref 1) and collinear phasematching were explored, and both methods yielded comparable spectra. For the collinear phasematching setup, the input beams (produced using a Spectraphysics MOPO 730 and home-built broadband OPO) were combined using a dichroic mirror and focused into the sample using a 20 cm FL achromatic lens. After the sample, KG3 and BG40 were used to absorb the broadband near-infrared input beams, and a holographic notch was angle-tuned to remove light from the tunable narrowband input beam (tuned in steps of 0.01 nm with 10 laser pulses per step).

Results and Discussion

Figures 3 and 4 show C2DRRS spectra of I_2 ($B^3\pi_u - X^1\Sigma_g$ transition) and C_2 ($d^3\pi_g - a^3\pi_u$). Iodine's relatively small vibrational frequency ($\omega_e' = 126$ cm^{-1}, $\omega_e'' = 214$ cm^{-1}) results in closely spaced cross-peaks, several of which fit into the (~18 nm wide) single exposure spectral window of the detection system. On the other hand, the large vibrational frequencies for C_2 ($\omega_e'' = 1641$ cm^{-1}, $\omega_e' = 1788$ cm^{-1}) produce wide spacings between cross-peaks. The C_2 results in Figure 4 therefore show selected portions of several C2DRRS spectra, along with a simulation to indicate their respective locations. Another difference between the C_2 spectra and the I_2 spectra is the direction and shape of the parabolas. The difference is due to the rotational constants; $B' < B''$ for I_2 but $B' > B''$ for C_2. The magnitude of this difference in C_2 is smaller than that in I_2, causing the C_2 parabola to be wider than that of I_2.[1]

The results indicate that the I_2 spectrum is dominated by the vibronic process. The parabola vertices align both vertically and horizontally, forming a series of rectangles. This pattern was found to repeat itself over a wide range of wavelengths throughout both the Stokes and anti-Stokes regions. Horizontal and vertical lines can be drawn through the parabola vertices, leading to a good approximation for the frequencies of the vibronic fundamental and overtones (the spacings between parabola correspond to the rotationless spacing between vibronic levels).

The dimensions of the rectangles vary slightly due to two factors: anharmonicity and the conversion from energy (or frequency) space to wavelength space. However, these effects are relatively small; for I_2, the anharmonicity changes the width and height of neighboring rectangles by a value of about 2 cm^{-1},

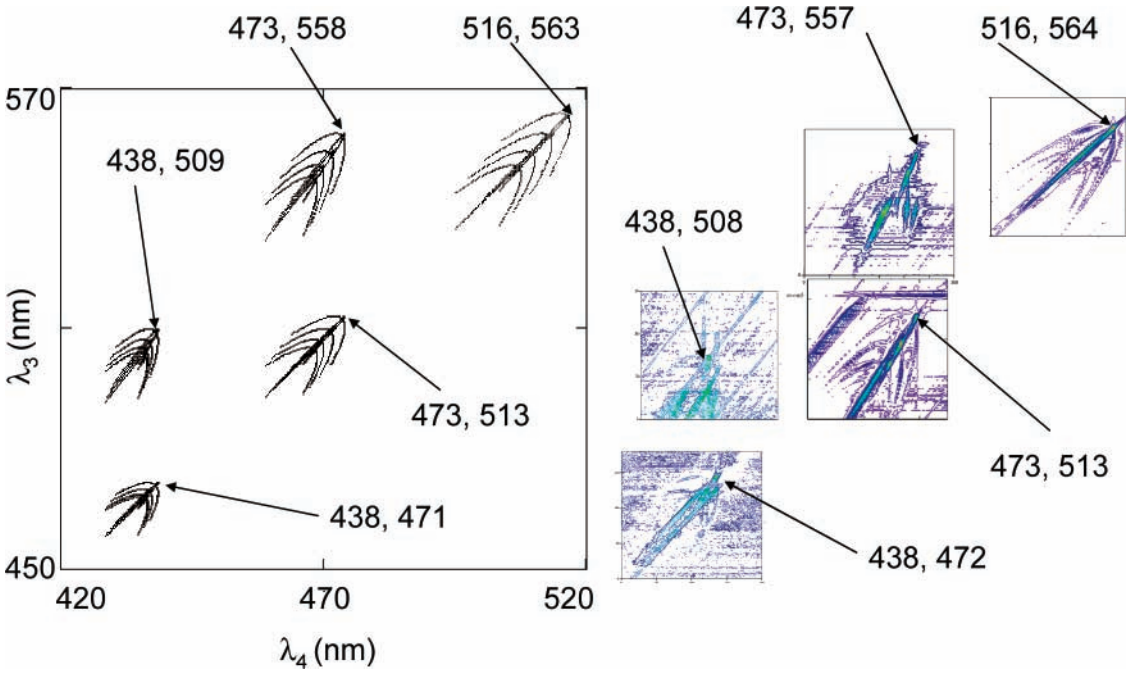

Figure 4. Simulated (left) and experimental (right) C2DRRS spectra of C_2. The simulated plot was generated using spectroscopic constants from the NIST website, and assumed that all transition dipole moments were equal in magnitude.[16] The relative size and spacings used for the experimental spectra are not consistent and not to scale.

or 3%. Changing from energy space to wavelength space changes the width and the height of neighboring rectangles by about 1%. The resulting combined effect for neighboring rectangles was found to be around 4%. Since these types of distortions only affect consistency in the spacing between the vertical and horizontal resonance lines (and not the slope of these lines), they do not cause the vibronic process to resemble the vibrational process. For I_2, the degree to which Δ_{da} is truly vertical was measured by comparing the positions of individual peaks within vertically adjacent parabolas. No deviation significantly greater than the resolution of the detection system ($\sim$0.01 nm) could be detected.

In Figure 4, the locations of the parabola clusters are labeled by the location of the upper right-hand vertices. The intensity and quality of the two $\Delta v'' = 2$ clusters (labeled 473, 558 and 438, 509) are weaker and poorer than that of the three other clusters that arise from $\Delta v'' = 1$. Nevertheless, the overall pattern is sufficiently clear to show that the parabola clusters align vertically but not horizontally; instead of resembling a rectangular grid, the pattern appears to resemble the parallelogram pattern characteristic of the vibrational process.

Both spectra show evidence of temperature-dependent population effects. In the vibronic process, the spacings between parabolas are influenced by only the vibronic levels, not the ground state vibrational levels. A thermally excited state process originating from the $v'' = 1$ level will produce a second rectangular grid identical to the $v'' = 0$ grid (if plotted in frequency space), but shifted to lower frequencies in both the x and y direction by a constant equal to the frequency of the ground-state fundamental. If $\omega_e' \approx \omega_e''$ and the anharmonicities are relatively small, then the location of all $v'' > 1$ parabolas will be very close to the location of $v'' = 0$ parabolas, shifted to lower frequency in both the x and y direction by the corresponding quanta of vibrational energy. This proximity occurs because the size of the shift depends on the frequency of the ground-state vibrational frequencies, while the size of the spacing between parabolas depends on the vibronic levels. For I_2, the considerable difference between the vibrational and vibronic constants results in a noticeable shift between the location of the $v'' = 0$ boxes and the $v'' = 1$ boxes shown in Figure 3.

Peaks from such thermally excited I_2 molecules at room temperatures are also commonly observed in conventional 1D absorption spectra of iodine. However, in the 1D spectra, the individual rovibrational peaks from the $v'' = 0$ and $v'' = 1$ levels can be difficult to distinguish and identify, especially in the 550−570 nm region where peaks from the two processes are of comparable strengths. The ability to cleanly resolve and easily distinguish these peaks in the C2DRRS spectrum illustrates one of benefits achieved by spreading information across a second dimension.

Unlike the vibronic spectra, which are insensitive to the $v'' \geq 1$ levels at low temperatures, the vibrational spectra are always influenced by the frequency of the $v'' \geq 1$ levels. The spacing between parabolas along the x axis (ω_4) depends on the vibronic frequencies. For the y axis (ω_3), however, the spacing depends on the difference between the vibrational and vibronic frequencies. If the vibrational and vibronic constants are similar, then some of these excited state doubly resonant points may be located in very close proximity to the doubly resonant points from the processes originating in the ground state. In the case of C_2, the high temperature of the flame and the similarity between ω_e' and ω_e'' cause the parabolas to cluster together into fingerprint-like patterns.

Under somewhat unusual circumstances, it might be difficult to determine whether the process is vibronic or vibrational. One example is the case where the vibrational and vibronic constants are identical (e.g., $\omega_e' = \omega_e''$). Another is the unusual case (e.g., temperature approaching infinity) where all vibrations in the ground state are equally populated.

Finally, this work also suggests a possible way to compare the Raman scattering activity of molecules in their ground and excited states. For example, the fact that iodine is consistently dominated by the vibronic processes (experimentally verified over a wide spectral range from $\omega_4 = 515$ to 567 nm) suggests that promoting the iodine molecule to its excited ($B^3\pi_u$) state raises its Raman scattering coefficients. In other words, this dominance of the vibronic process could be explained if $\langle c|\mu|e\rangle \langle e|\mu|d\rangle$ is substantially greater than $\langle a|\mu|e\rangle \langle e|\mu|b\rangle$. (Note that the transition dipole moment μ_{da} appears in both vibrational and vibronic expressions, and μ_{bd} and μ_{ac} contain identical elements or elements that are similar in magnitude.) The same arguments suggest that promoting the C_2 molecule from the $a^3\pi_u$ state to the $d^3\pi_g$ state decreases its Raman scattering properties.

Conclusion

The interpretation of conventional spectra can be complicated by the existence of multiple processes that involve different selection rules, a variety of types of levels (electronic, vibrational, and rotational), and a large range of possible quantum numbers. Conventional spectroscopy is restricted to one dimension, which limits the amount of information and the ability to use pattern recognition. Not only is it challenging to match peaks to their respective process, but it is also not obvious what type of processes produce the resulting spectra. By using an additional dimension, C2DRRS can provide a means for sorting peaks according to rotational and vibrational quantum number, vibrational sequence, and rotational selection rule. This paper extends this capability by demonstrating how pattern recognition in two-dimensional spectroscopy can be used to immediately distinguish resonantly enhanced processes that probe the ground electronic state from those that probe the excited electronic state.

Acknowledgment. This work was supported by the National Science Foundation (Grants No. CHE-0215878 and EEC-0310717). Additional support was provided by the NIH (Grant No. MD-02-005 and 2G11HD037062).

References and Notes

(1) Chen, P. C.; Joyner, C. C. *Anal. Chem.* **2005**, *77*, 5467−5473.
(2) Brixner, T.; Stenger, J.; Vaswani, H. M.; Cho, M.; Blankenship, R. E.; Fleming, G. R. *Nature* **2005**, *434*, 625−628.
(3) Jonas, D. M. *Annu. Rev. Phys. Chem.* **2003**, *54*, 425−463.
(4) Wright, J. C. *Int. Rev. Phys. Chem.* **2002**, *21*, 185−255.
(5) Mukamel, S. *Annu. Rev. Phys. Chem.* **2000**, *51*, 691−729.
(6) Khalil, M.; Demirdoven, N.; Tokmakoff, A. *J. Chem. Phys.* **2004**, *121*, 362−373.
(7) Noda I.; Ozaki, Y. *Two-Dimensional Correlation Spectroscopy, Applications in Vibrational and Optical Spectroscopy*; Wiley-Interscience: Chichester, England, 2004.
(8) Aue, W. P.; Bartholdi, B.; Ernst, R. R. *J. Chem. Phys.* **1976**, *64*, 2229.
(9) Meyer, K. A.; Besemann, D. M.; Wright, J. C. *Chem. Phys. Lett.* **2003**, *381*, 642−649.
(10) Zanni, M. T.; Ge, N.-H.; Kim, Y. S.; Hochstrasser, R. M. *Proc. Natl. Acad. Sci. U.S.A.* **2001**, *98*, 11265−11270.
(11) Golonzka, O.; Khalil, M.; Demirdöven, N.; Tokmakoff, A. *Phys. Rev. Lett.* **2001**, *86*, 2154−2157.
(12) Prior, Y.; Bogdan, A. R.; Dagenais, M.; Bloembergen, N. *Phys. Rev. Lett.* **1981**, *46*, 111−114.

(13) Andrews, J. R.; Hochstrasser, R. M. *Chem. Phys. Lett.* **1981**, *83*, 427−431.
(14) Aben, I.; Ubachs, W.; van der Zwan, G.; Hogervorst, W. *Optics Commun.* **1993**, *95*, 97−102.
(15) Chen, P. C.; Joyner, C. C. *Journal Mol. Struct.*, in press.
(16) Huber, K. P.; Herzberg, G. "Constants of Diatomic Molecules" in *NIST Chemistry WebBook, NIST Standard Reference Database Number 69*; P. J. Linstrom, P. J., Mallard, W. G., Eds.; National Institute of Standards and Technology: Gaithersburg, MD, March 2003; (http://webbook.nist.gov).